nature communications

Article

https://doi.org/10.1038/s41467-025-68209-y

Volumetric compression regulates the phase separation of AXIN and acts as an operational amplifier to bidirectionally modulate Wnt signaling in organoids

Received: 9 April 2025

Accepted: 22 December 2025

Published online: 08 January 2026

Check for updates

Jinyun Shi[1], Linze Wu[1], Pengjie Li[1], Fukang Qi[1], Mengcheng Lei[1], Xueqing Ren[1], Han Xie[1], Wenhui Wang[1], Yi Zheng[2,3,4], Peng Chen[1], Limin Xia[5], Chen Shi[6], Yu Zhang[6], Bi-Feng Liu[1] & Yiwei Li[1]

Protein phase separation has emerged as a crucial mechanism for spatio-temporal regulation of intracellular processes, yet its potential to integrate and compute diverse extracellular signals is not fully understood. Here, we show a mechano-biochemical circuit that harnesses phase separation to process mechanical and biochemical inputs, modulating cell fate decisions. We demonstrate that volumetric compression bidirectionally regulates canonical Wnt/β-catenin signaling, where the presence of Wnt ligands determines the locations of AXIN phase separation to form either LRP6 signalosomes on the cell membrane or β-catenin destruction complexes in the cytosol, while the mechanical stimulus promotes degree of phase separation to amplify either the positive or negative signal. This circuit enhances healthy intestinal organoid proliferation while suppressing patient-derived colorectal cancer organoid growth, revealing its potential for precise mechanotherapy. Our findings establish phase separation as a critical component in mechanical signal transduction and provide a framework for integrating mechanical and biochemical cues in cellular decision-making. This approach opens avenues for targeted therapies and deepens our understanding of how cells process complex environmental information.

In multicellular organisms, human cells are subjected to dynamic mechanical cues in both healthy and diseased tissues[1–5]. The incorporation of mechanical cues in biological processes is essential for maintaining homeostasis in healthy tissues, while their dysregulated introduction leads to diseases[6]. For instance, dermal progenitors aggregate through contractility-driven cellular pulling to trigger the mechanosensitive activation of β-catenin in adjacent epidermal cells until follicle pattern formation[7]; aging-induced niche stiffening hinders the function of oligodendrocyte progenitors (OPCs) by activating PIEZO1 signaling[8]; tumor-induced compressive stresses reprogram

[1]The Key Laboratory for Molecular Biophysics of MOE—Hubei Bioinformatics and Molecular Imaging Key Laboratory, Department of Biomedical Engineering, College of Life Science and Technology, Huazhong University of Science and Technology, Wuhan, China. [2]Hubei Provincial Hospital of Traditional Chinese Medicine, Wuhan, China. [3]Affiliated Hospital of Hubei University of Chinese Medicine, Wuhan, China. [4]Hubei Province Institute of Traditional Chinese Medicine, Wuhan, China. [5]Department of Gastroenterology, Hubei Key Laboratory of Hepato-Pancreato-Biliary Diseases, Institute of Liver and Gastrointestinal Diseases, Tongji Hospital of Tongji Medical College, Huazhong University of Science and Technology, Wuhan, Hubei, China. [6]Department of Pharmacy, Union Hospital, Tongji Medical College, Huazhong University of Science and Technology, Wuhan, China. e-mail: yiweili@hust.edu.cn

adjacent adipocytes via the activation of Wnt/β-catenin signaling[9]. Despite of the reported mechanisms in understanding mechanoregulation[10], the interplay between mechanical perturbations and biochemical signaling is still complex and elusive, with both promotional and inhibitory effects reported across different biological systems[11–13]. For instance, pressure from tumor growth induces tumorigenic β-catenin to elevate the expression of Wnt target genes in the intestinal epithelium[12], while stretching has been reported to inhibit Wnt/β-catenin signaling in mineralizing osteoblasts[14]. This may be attributed to different forms of mechanical loads and varying biological contexts, which urges a framework to understand the crosstalk between mechanoregulation and biochemical signaling pathways as an integrated system for understanding diverse biological outcomes.

The current paradigm for understanding mechanical signaling transduction involves exploring the impact of mechanical cues on classic biochemical signaling pathways, such as Wnt signaling, Hippo pathway, BMP signaling, and Notch signaling, via specific responsive proteins[13,15–18]. Various patterns or modules in mechanoregulation have been discovered, including cell surface mechanotransducers[19], mechanoresponsive ion channels[20], nuclear translocations of transcription factors[21], nuclear deformation[22], and changes of chromatin dynamics[23]. In addition to these findings, our previous research and a few other studies present a framework where biomolecular condensates via phase separation sense intracellular molecular crowding caused by water efflux under mechanical stress, altering their phase separation states to affect signaling transduction[13,22]. While protein phase separation has recently been highlighted as a critical player in cells to spatiotemporally govern intracellular processes, yet the understanding of its role has mostly been limited to process individual stimuli. Instead, we propose that a biomolecular circuit built upon phase separation mechanism is able to process a combinatory of hybrid stimuli from both biochemical and mechanical environments.

Towards this end, we hypothesize that a framework circuit can integrate the bi-directional outcomes of a certain mechanical cue on cell fate decisions via regulating Wnt/β-catenin signaling, which is one of the essential pathways controlling cell fate in various biological systems, including embryonic stem cells, mesenchymal stem cells, intestinal stem cells, and neuron progenitors[23]. This is reminiscent of genetic circuit, which is an application of synthetic biology where biological parts inside a cell are designed to perform logical functions mimicking those observed in electronic circuits, which enables cells to respond and compute multiple informations for cellular decisions[24–26]. Examples of genetic circuits include genetic logic gates, cascades, bandpass filters, switches, and memory[27] for regulating circadian clocks, cell divisions[28], and cell fate decision[26,29,30]. Whether mechanotransduction and biochemical signaling work together in an architecture similar to circuits in synthetic biology remains elusive. If such a mechano-biochemical circuit exists, how it performs and its consequences for biological systems still need to be explored.

Here, we report the mechano-biochemical circuit that integrates mechanical and biochemical signals to modulate cell fate decisions. Specifically, we demonstrate that volumetric compression interacts with the Wnt ligand to create an operational amplifier (op amp)-like function on canonical Wnt/β-catenin signaling. This circuit leverages the phase separation of AXIN puncta to receive and process information from both mechanical cues and biomolecular ligands, leading to outputs of either promotion or inhibition. Our findings further reveal that this circuit can differentially regulate the growth of healthy intestinal organoids (promotion) and colorectal cancer (CRC) organoids (inhibition) with a single input of volumetric compression. This circuit provides a framework for understanding mechanoregulation and offers avenues for developing therapies that precisely target cell fate decisions. By integrating mechanical and biochemical cues, our study paves the way for potential applications in regenerative medicine and cancer therapy.

Results

Translocated phase separation of AXIN enables the mechano-biochemical circuit for formation of two distinct membraneless organelles

Our previous study revealed that volumetric compression, as one of the mechanical cues, can promote Wnt/β-catenin signaling by stabilizing the LRP6-AXIN signalosome[13]. The formation of the LRP6-AXIN complex requires AXIN's ability to undergo phase separation or head-to-tail polymerization[31]. In the absence of the Wnt ligand, AXIN still undergoes phase separation and puncta formation in the cytoplasm[32,33]. In the cytoplasm, AXIN co-localizes with adenomatous polyposis coli (APC) to form the β-catenin destruction complex, which degrades cytosolic β-catenin to maintain a low basal level of Wnt/β-catenin signaling[32,33]. Given that the promoting effect of volumetric compression on Wnt/β-catenin signaling relies on the phase separation of AXIN with LRP6 at the cell membrane[13], we speculate that volumetric compression can also negatively regulate Wnt/β-catenin signaling in the absence of the Wnt ligand. Therefore, we hypothesize that volumetric compression can bidirectionally regulate Wnt/β-catenin signaling with the assistance of AXIN phase separation (Fig. 1a). This regulation circuit can be viewed as an op amp, an analog circuit block that takes a differential voltage input and produces a single-ended voltage output. Basically, the op amp can amplify weak electric signals from two different inputs. The difference is that one input inverts the signal in the opposite direction (i.e.: the signal is out of phase by 180 degrees in output), while the other does not. The operational amplifier can switch to each of its inputs. In our model, whether the Wnt ligand is presented determines the switch between two inputs, while the volumetric compression amplifies the strength of the signal (Fig. 1a). Given the involvement of Wnt/β-catenin signaling in many biological processes across multiple scales, this op amp-like circuit can be incorporated into many biological regulations.

To test our hypothesis, we constructed both phase-separable WT AXIN-mCherry and AXINΔDAX-mCherry with compromised phase separation capability in mammalian AXIN1 knockout (KO) 293 T cells and RKO cells (Supplementary Fig. 1a). RKO cells have no intrinsic β-catenin transcriptional activity, due to the lack of either endogenous Wnt ligands or membrane cadherin-catenin complex; meanwhile, despite the fact that HEK293T cells have membrane β-catenin, their autocrine WNT ligands are limited, which is confirmed by our ELISA assays (Supplementary Fig. 1b), making it hard to trigger downstream signalosome formation and β-catenin accumulation. Then, we tested the phase separation behavior of AXIN puncta in these cells. The FRAP assays (Fig. 1b), along with live imaging of AXIN puncta splitting (Fig. 1c) and fusion (Fig. 1d), confirmed the dynamic exchange of AXIN proteins within puncta structures and their liquid-like behavior in the cytoplasm. AXIN puncta were consistently observed in WT AXIN cells, while AXINΔDAX-mCherry compromised the formation of AXIN puncta[31,34–36].

Next, we compared the effect of volumetric compression on the condensate formation of AXIN with or without the DAX domain (Fig. 1e). For WT AXIN-mCherry, volumetric compression enriched a larger portion of AXIN into condensates (Fig. 1f) and increased the number of condensates formed by WT AXIN (Fig. 1g). This effect was also confirmed with endogenous AXIN using immunostaining (Fig. 1h), showing a larger portion of AXIN in condensates (Fig. 1i). In contrast, the impact of volumetric compression on AXIN-ΔDAX-mCherry condensates was limited (Fig. 1e); no significant increase in the number of AXIN condensates was found (Supplementary Fig. 1c), nor was there a change in the proportion of AXIN in condensates relative to cytoplasmic AXIN (Supplementary Fig. 1d).

Next, we explored whether the effect of volumetric compression on AXIN condensates directed the formation of functional membraneless organelles regulating Wnt/β-catenin signaling. Without the Wnt ligand, AXIN mostly localized in the cytoplasm, where it merged with

https://doi.org/10.1038/s41467-025-68209-y

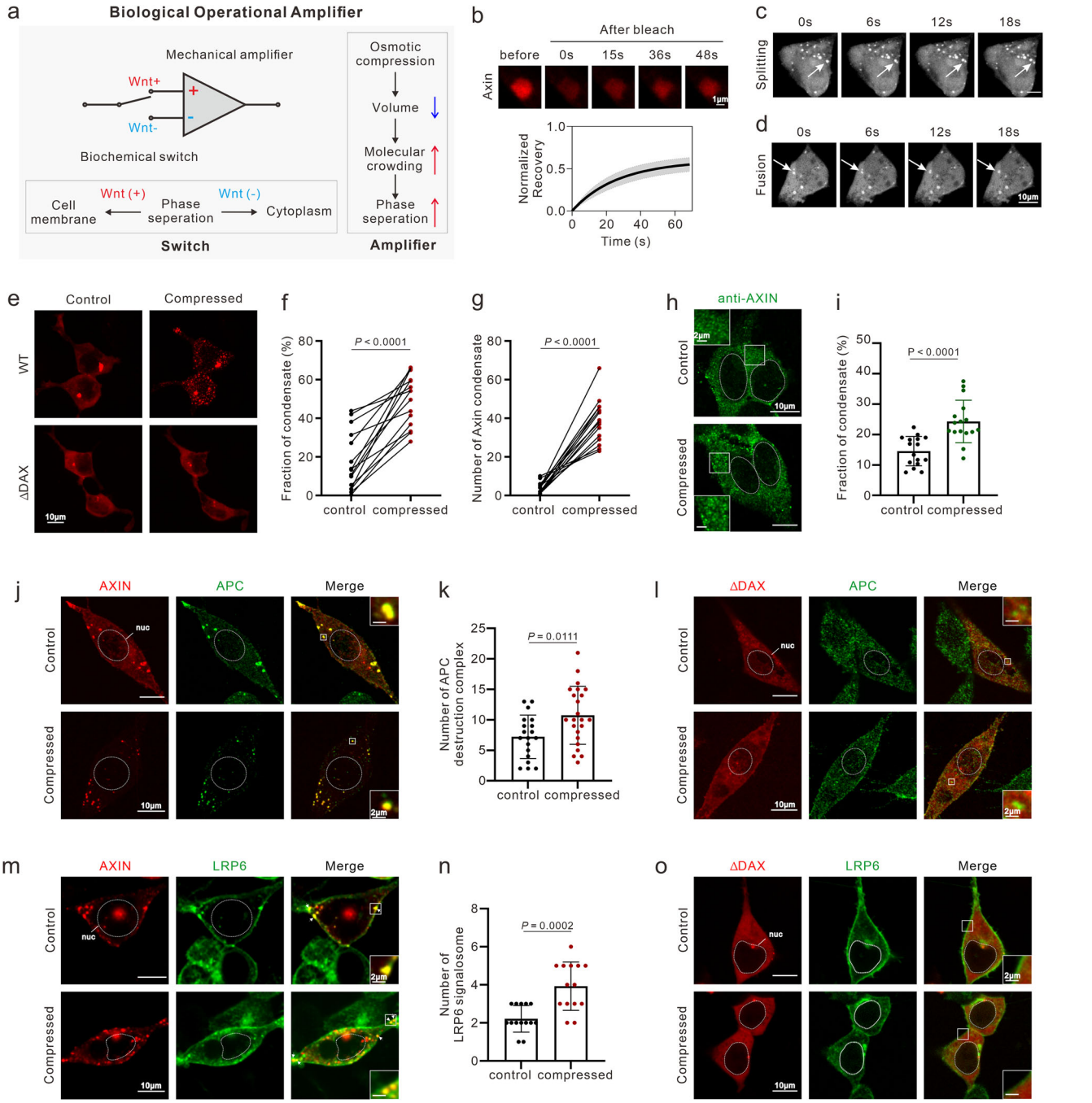

Fig. 1 | A mechano-biochemical operational amplifier circuit guiding formation of two distinct membraneless organelles based on translocated phase separation. a Schematic illustration of a mechano-biochemical operational amplifier that operates via combinational inputs of Wnt ligand and volumetric compression. **b** FRAP assay showing the recovery of AXIN condensates after photobleaching. Data are presented as mean ± s.d. ($n = 7$ biologically independent experiments). Scale bar, 1 µm. Representative images showing the splitting (**c**) and fusion (**d**) of AXIN droplets formed inside a cell. White arrows indicate the splitting or fusing droplets. Images are representative of three independent experiments with similar results. Scale bar, 10 µm. Volumetric compression promotes the formation of AXIN-mCherry condensates inside cells ($n = 15$ cells) (**e**), as indicated by either the fraction of total AXIN in condensates (**f**) or the number of AXIN condensates (**g**). The effect was suppressed upon DAX domain deletion in the AXIN protein (**e**). Scale bar, 10 µm. In **f** and **g**, data are presented as mean ± s.d. and were analyzed by two-tailed paired *t*-test. Volumetric compression promotes the formation of endogenous AXIN condensates inside cells (**h**) by fluorescent immunostaining, as indicated by the fraction of total AXIN in condensates ($n = 16$ cells per group) (**i**). **j**–**l** Volumetric compression promotes the assembly of the APC destruction complex (co-localized puncta of AXIN and APC) inside cells (**j**), quantified by the number of APC destruction complexes per cell (control, $n = 20$; compressed, $n = 23$ cells) (**k**). This effect was suppressed upon DAX domain deletion (**l**). **m**–**o** Volumetric compression promotes the formation of LRP6 signalosomes (co-localized puncta of AXIN and LRP6) inside cells (**m**), quantified by the number of LRP6 signalosomes per cell ($n = 14$ cells per group) (**n**). This effect was suppressed upon DAX domain deletion (**o**). In **h**, **j**, **l**, **m**, **o**, dotted circles indicate the location of the cell nucleus. Scale bars, 10 µm (main field). The white boxed regions are magnified and shown on the left or right. Scale bar, 2 µm. In **i**, **k**, **n**, data are presented as mean ± s.d. and were analyzed by two-tailed unpaired *t*-test. Exact *p* values are shown in the figure. Source data are provided as a Source Data file.

APC to form the β-catenin destruction complex[37]. This complex is a critical tumor-suppressing membraneless organelle that maintains a consistently low level of cytoplasmic β-catenin by triggering its ubiquitination. Mutations or deletion of essential components in the β-catenin destruction complex can initiate colorectal cancers (CRCs)[37]. Stabilizing the β-catenin destruction complex holds the potential for suppressing tumor growth[33,37]. Our results showed many β-catenin destruction complexes with co-localized AXIN and APC forming yellow dots in the images (Fig. 1j). Under volumetric compression, the number of β-catenin destruction complexes, indicated by yellow spots, increased further (Fig. 1j, k). Quantitative analysis showed a 40% increase in β-catenin destruction complexes under volumetric compression (Fig. 1k). Meanwhile, without Wnt ligands, AXIN does not translocate to the membrane, no obvious colocalization between AXIN and LRP6 can be observed (Supplementary Fig. 2a). We also verified that the DAX domain mediated the phase separation-like formation of β-catenin destruction complexes (Fig. 1l). Deletion of the DAX domain disrupted the colocalization of APC and AXIN proteins, and prevented the promotion effect of volumetric compression on assembly of β-catenin destruction complexes in response to volumetric compression (Fig. 1l and Supplementary Fig. 1e, f).

In the presence of Wnt, the Wnt ligand triggers the phosphorylation of LRP6, which recruits AXIN from the cytoplasm to the cell membrane to form the LRP6 signalosome and initiates Wnt signaling transduction from the cell membrane into the cell[38,39]. When Wnt3a ligands were introduced to cultured cells, we observed the formation of LRP6 signalosomes as yellow condensates beneath the cell membrane (Fig. 1m). With additional volumetric compression, the number of LRP6 signalosomes nearly doubled (Fig. 1n). Interestingly, the effect of volumetric compression on the LRP6 signalosome was also mediated by the phase separation-like behavior controlled by the DAX domain within AXIN molecules (Fig. 1o); with the DAX domain deleted, the co-localization between LRP6 and AXIN proteins was weakened and no promotional effect of volumetric compression on the LRP6 signalosome formation existed (Fig. 1o and Supplementary Fig. 1g, h). Meanwhile, in presence of WNT ligands, we observe minimal cytoplasmic condensates showing AXIN-APC colocalization (Supplementary Fig. 2b). Nevertheless, we found that some residual AXIN-APC interaction persist in the cytoplasm, consistent with other literatures[40,41]; this is because the Wnt activation will not recruit all the cytoplasmic AXIN, but instead to compromise the capability of the APC destruction complex to degrade β-catenin to accumulate cytoplasmic β-catenin.

Together, the results showed that the condensate formation capability of AXIN via its DAX domain enabled a mechano-biochemical circuit that bidirectionally controlled the formation of two distinct membraneless organelles within Wnt/β-catenin signaling. In the presence of Wnt ligands, volumetric compression promoted the formation of the LRP6 signalosome, while in their absence, volumetric compression promoted the formation of the β-catenin destruction complex instead.

The mechano-biochemical circuit regulates canonical Wnt/β-catenin signaling

Given the importance of two distinct membraneless organelles that regulate Wnt/β-catenin signaling, we speculated that the mechano-biochemical circuit also regulated canonical Wnt/β-catenin signaling.

To verify our hypothesis, we tested either the activation or inhibition of canonical Wnt/β-catenin signaling generated by volumetric compression under different conditions. AXIN can bind to either β-catenin or LRP6: when AXIN binds with β-catenin, β-catenin undergoes ubiquitination and degradation, decreasing Wnt/β-catenin signaling[41]; when AXIN binds to LRP6, the degradation of β-catenin mediated by the APC destruction complex is inhibited, leading to the accumulation of β-catenin and an increase in Wnt/β-catenin signaling[40]. Thus, the mechano-biochemical circuit switches to the inverting input to promote AXIN-β-catenin binding when the Wnt ligand is absent; while switching to the non-inverting input, when the Wnt ligand is present, to promote AXIN-LRP6 binding. To test this model, Co-immunoprecipitation (Co-IP) assays were performed. In the absence of Wnt ligands, IP assays showed that volumetric compression increased the amount of β-catenin bound to AXIN (Fig. 2a, b), suggesting more β-catenin might be degraded under volumetric compression. In the presence of Wnt ligands, IP assays showed that volumetric compression doubled the amount of LRP6 bound to AXIN (Fig. 2c, d), suggesting potential accumulation of β-catenin in the cytoplasm; accordingly, we also confirmed that the binding ratio between AXIN and APC decreased (Supplementary Fig. 2c, d). These two bidirectional effects were also dependent on the DAX domain. Deletion of the DAX domain in AXIN eliminated the observed bidirectional promotion effects on protein binding (Fig. 2a–d).

Next, we directly assessed the accumulation of β-catenin with different combinations of volumetric compression and Wnt3a ligand stimulation using immunostaining assays[42]. In most cases, the basal level of β-catenin is relatively low, and a further decrease might have a minor impact on cell functions and downstream gene expression. However, β-catenin can also be increased independently of Wnt ligands and phosphorylated LRP6, such as in pathological accumulations of β-catenin resulting from mutations in APC, glycogen synthase kinase-3 (GSK-3), and β-catenin itself[43,44]. Suppression of such pathological accumulations of β-catenin can be a therapeutic target for treating diseases like colorectal cancers (CRCs)[45]. We used CHIR to accumulate β-catenin independently of Wnt ligands and LRP6 by inhibiting GSK3, a kinase that leads to the degradation of β-catenin[46]. CHIR99021 is a highly specific GSK-3β inhibitor that prevents β-catenin phosphorylation and subsequent degradation, thereby stabilizing cytoplasmic β-catenin through a mechanism that completely bypasses the need for Wnt ligand-LRP5/6 receptor engagement[46,47]. In this case, even though cytosolic β-catenin increased, volumetric compression still decreased the amount of cytosolic β-catenin in the absence of Wnt ligands (Fig. 2e, f). This suggests potential applications of volumetric compression to inhibit the pathological accumulation of β-catenin in diseases.

Additionally, we also tested the impact of volumetric compression on β-catenin in the presence of Wnt ligands. Indeed, the results showed that Wnt3A induced the accumulation of cytosolic β-catenin, which was further augmented by volumetric compression (Fig. 2h, i). Thus, the mechano-biochemical circuit can augment β-catenin in the canonical pathway and suppress pathological accumulation of β-catenin with designed combinations of Wnt ligands and volumetric compression. Again, this mechano-biochemical circuit's effect on both canonical and pathological accumulations of β-catenin could be eliminated by removing the DAX-driven phase separation of AXIN condensates (Fig. 2e, g, h, j). Western blot assays also supported the DAX domain as the hub for constructing this mechano-biochemical circuit and produced consistent results that various combinations of Wnt ligands and volumetric compression diverted the accumulation or degradation of β-catenin (Fig. 2k, l).

Since the accumulation of β-catenin leads to the gene expression of Wnt target genes, which is key to drive long-term cell fate decisions, we further used RT-qPCR assays to verify the regulation of the mechano-biochemical circuit at the gene expression level. In the absence of Wnt ligands, volumetric compression suppressed the basal expression of key Wnt target genes, including *AXIN2*, *LEF1*, and *SP5* (Fig. 2m). Conversely, in the presence of Wnt ligands, compression further enhanced the expression levels of all three genes (Fig. 2n). Moreover, the effect of volumetric compression in both conditions (with or without Wnt ligands) was eliminated by the deletion of the DAX domain in AXIN (Fig. 2o, p).

https://doi.org/10.1038/s41467-025-68209-y

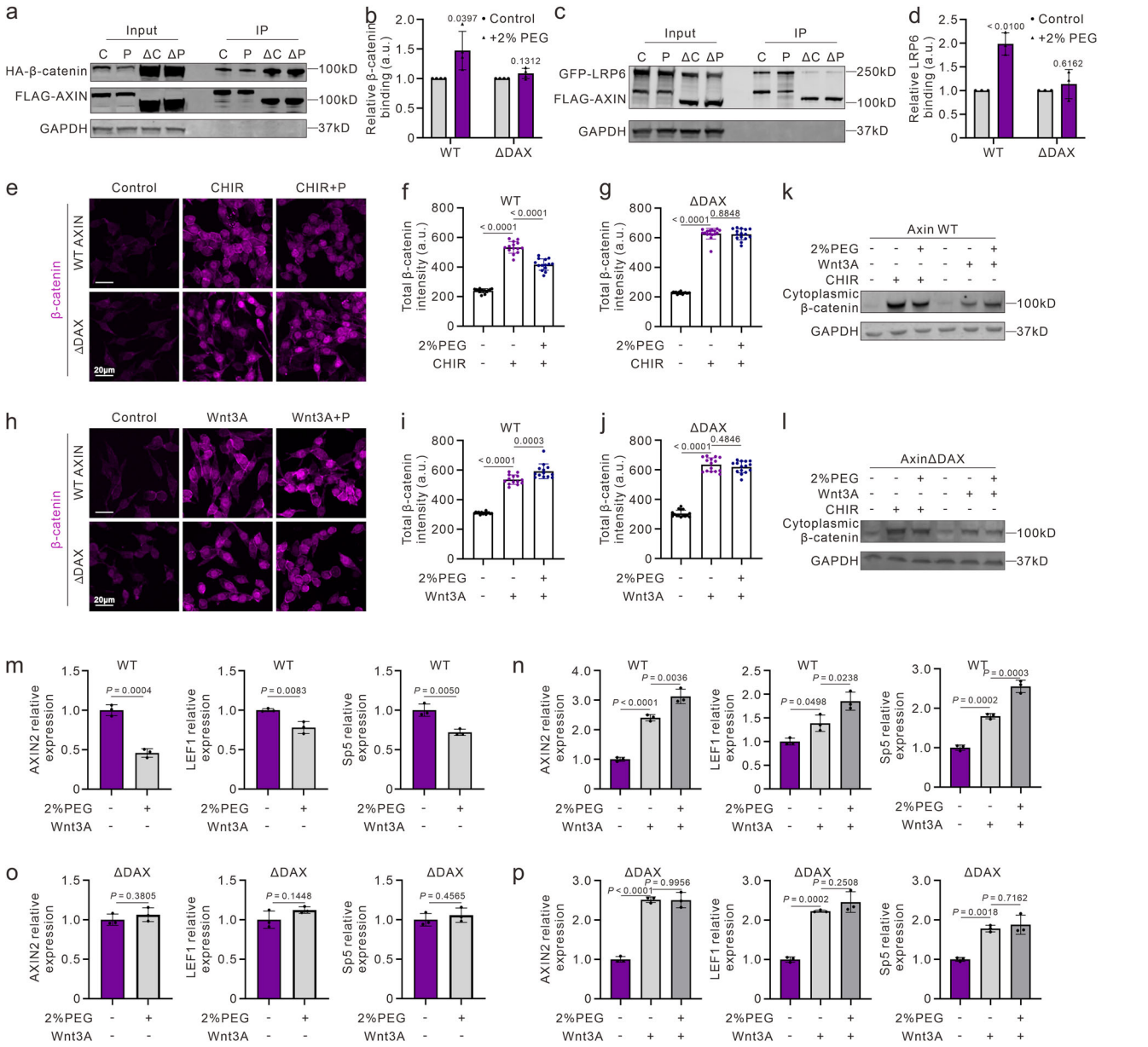

Fig. 2 | A mechano-biochemical operational amplifier circuit guiding distinct outputs of AXIN-β-catenin binding, β-catenin accumulation, and Wnt/β-catenin signaling activation. Western blot showing that volumetric compression promotes AXIN binding β-catenin (**a**; quantified in **b**) and LRP6 (**c**; quantified in **d**). These effects were abolished upon DAX domain deletion. **e**–**g** RKO cells treated with CHIR99021 (3 μM) show β-catenin degradation under compression (**e**), quantified in (**f**) ($n = 14$ cells per group). This degradation was prevented upon DAX domain deletion (control, $n = 15$; CHIR, $n = 16$; CHIR + 2P, $n = 15$ cells) (**e**, **g**). Scale bar, 20 μm. **h**–**j** Immunostaining shows compression leads to β-catenin accumulation under Wnt3a stimulation (**h**), quantified in (**i**) (control, $n = 14$; Wnt3A, $n = 14$; Wnt3A + 2P, $n = 13$ cells). This was prevented upon DAX domain deletion ($n = 15$ cells per group) (**h**, **j**). Scale bar, 20 μm. Western blot analysis showing that volumetric compression results in β-catenin degradation in the absence of Wnt ligands but accumulation in the presence of Wnt ligands (**k**), the bidirectional regulation on β-catenin is eliminated upon DAX domain deletion (**l**). Data are representative of three independent experiments with similar results. RT-qPCR showing that compression inhibits the expression of Wnt target genes *AXIN2*, *LEF1*, and *SP5* in the absence of Wnt ligands (**m**), while elevating their expression in the presence of Wnt ligands (**n**). RT-qPCR showing that the inhibitory (**o**) or promotive (**p**) effects of volumetric compression on Wnt target gene expression are prevented upon DAX domain deletion. In **b**, **d**, data are presented as fold change relative to the respective control group (set to 1). Statistical significance was determined using a two-sided ratio paired *t*-test on raw densitometry values ($n = 4$ independent experiments for **b**; $n = 3$ independent experiments for **d**). In **f**, **g**, **i**, **j**, data are presented as mean ± s.d. and were analyzed by one-way ANOVA. In **m**–**p**, data are representative of three independent experiments ($n = 3$ per group); data are presented as mean ± s.d. and were analyzed by two-tailed unpaired *t*-test. Exact *p* values are shown in the figure. a.u. arbitrary units. Source data are provided as a Source Data file.

Overall, given its capability for regulation of canonical Wnt/β-catenin signaling at both the protein and gene expression levels, the mechano-biochemical circuit functions as an op amp to either inhibit or elevate Wnt/β-catenin signaling, holding potential for engineering and diverting cell fate in distinct biological systems.

The mechano-biochemical circuit diverts cell fate of organoids from intestinal epithelium

Here, we further explored the incorporation of the mechano-biochemical circuit in engineering multicellular living systems, including healthy mouse intestinal organoids and human patient-

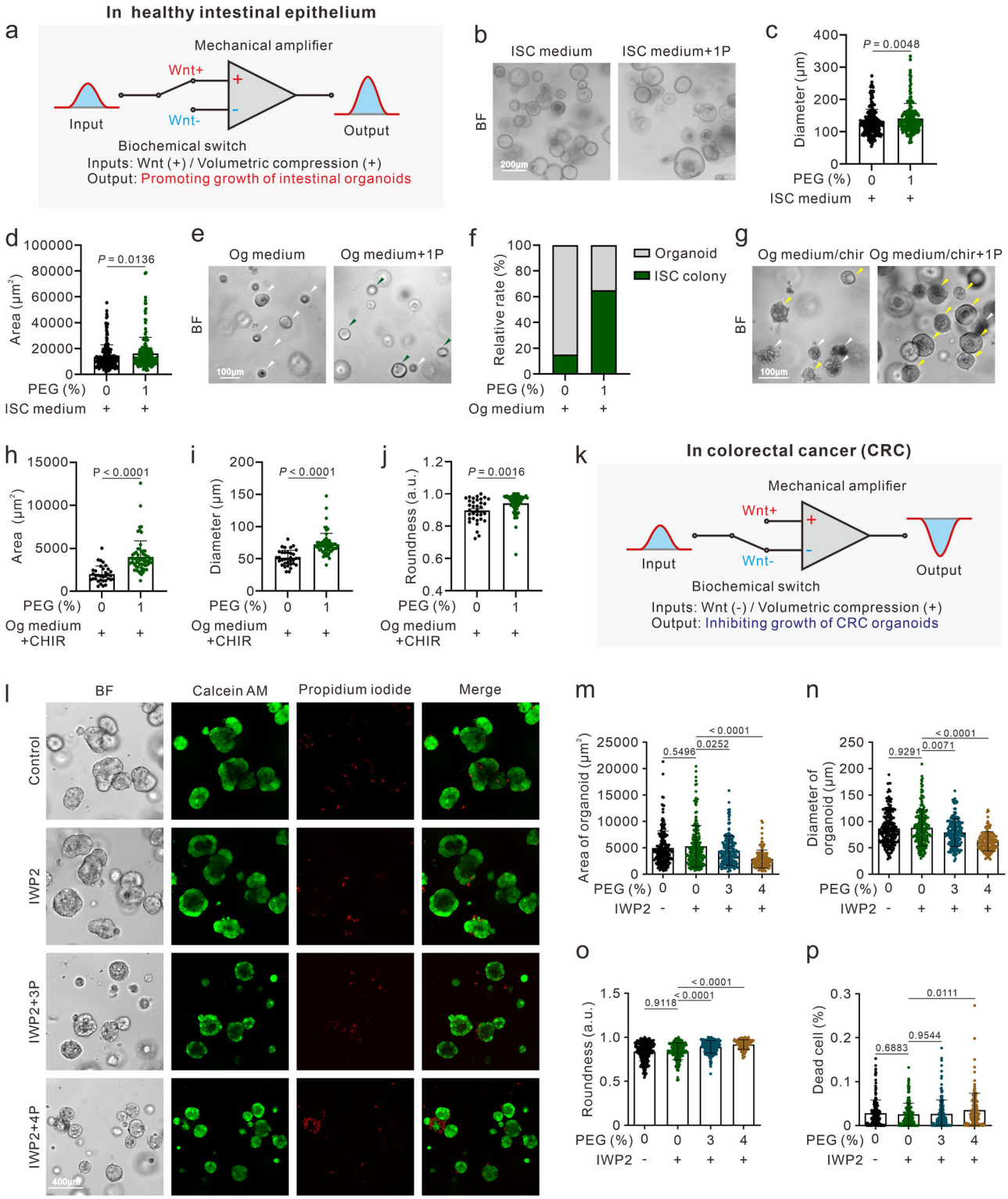

derived CRC organoids. In intestinal organoids, Lgr5+ intestinal stem cells (ISCs) self-renew when maintaining high-level Wnt/β-catenin signaling and further organize cells into crypts and villi in vivo and into intestinal organoids in vitro[48]. The activation of Wnt/β-catenin signaling is maintained by Wnt ligands from either mesenchyme or Paneth cells in the intestinal epithelium in vivo and by extraneous Wnt ligands or R-spondin (a Wnt signaling amplifier) in the medium for organoids in vitro[49–51]. When canonical Wnt/β-catenin signaling is suppressed, the intestinal epithelium/organoids undergo differentiation, eventually leading to apoptosis[52]. Given the bidirectional effect of the mechano-biochemical circuit, we anticipated a potential impact of volumetric compression on the growth and fate decision of intestinal organoids.

Since the presence of Wnt ligands is essential for the growth of intestinal organoids, we suggested that the mechano-biochemical circuit worked with a non-inverting input switch-on to promote the growth of organoids (Fig. 3a). We hypothesized that volumetric compression would augment canonical Wnt/β-catenin signaling and eventually affected the growth of intestinal organoids. Thus, we respectively cultured murine ISC organoids and crypt intestinal

Fig. 3 | A mechano-biochemical operational amplifier circuit guides distinct cell fate decisions in healthy intestinal organoids and colorectal cancer organoids. **a** Schematic illustration showing that in healthy intestinal epithelium or organoids, Wnt/β-catenin signaling is required for cell growth. The operational amplifier switches to "non-inverting input", promoting the growth of healthy intestinal organoids. **b**–**d** ISC spheroids were cultured in ISC medium with Wnt ligands. Representative images showing that volumetric compression generates larger ISC spheroids (**b**), consistently supported by quantifications of diameters (**c**) and areas (**d**) (Control, $n = 199$; Compressed, $n = 175$ organoids). Scale bar, 200 μm. **e**, **f** Organoids were cultured in Organoid (Og) medium. Representative images showing that compression promotes the transition to ISC colonies (**e**), quantified by the relative rate of colony formation (**f**) ($n = 100$ organoids). Scale bars, 100 μm. **g**–**j** Intestinal organoids were cultured in Og medium with CHIR99021. Representative images showing that compression promotes organoid growth (**g**), quantified by area (**h**), diameter (**i**), and roundness (**j**) (Control, $n = 34$; Compressed, $n = 63$ organoids). Scale bar, 100 μm. **k** Schematic illustration showing that in colorectal cancer (CRC), Wnt/β-catenin signaling is typically hyperactivated with pathological β-catenin accumulation. The operational amplifier switches to "inverting input", inhibiting CRC organoid growth. **l** CRC organoids were cultured in CRC medium with IWP2 (to exclude possible Wnt ligands) or osmotic compression (3% or 4% PEG 300). Representative images showing that IWP2 does not affect growth, whereas compression inhibits growth. Scale bar, 400 μm. Quantifications showing that volumetric compression reduces the area (**m**), diameter (**n**), and alters the morphology (**o**) of CRC organoids, with no significant effect on cell viability at 3% PEG and only a minimal effect at 4% PEG (**p**). (Control, $n = 204$; IWP2, $n = 201$; 3% PEG, $n = 185$; 4% PEG, $n = 137$ organoids). In **b**, **e**, **g**, **l**, data are representative of three independent experiments with similar results. In **c**, **d**, **h**–**j**, data are presented as mean ± s.d. and were analyzed by two-tailed unpaired *t*-test. In **m**–**p**, data are presented as mean ± s.d. and were analyzed by one-way ANOVA. Exact *p* values are shown in the figure. Source data are provided as a Source Data file.

organoids with or without volumetric compression (supplemented with 1% PEG 300). Indeed, we observed a promotive effect of volumetric compression on the growth of ISC organoids (Fig. 3b), as shown by both their areas and diameters (Fig. 3c, d). Additionally, this promotion effect was more obvious on crypt intestinal organoids (Fig. 3e) with Organoid (Og) medium. The reason could be that the Wnt/β-catenin signaling in ISC organoids is already near saturation due to the over-supplied Wnt ligands, but the Wnt/β-catenin signaling in intestinal organoids is largely dependent on the endogenous Wnt ligand, leaving space for further augmenting. A result was that the volumetric compression resulted in a large portion of crypt intestinal organoids transiting into spherical organoids (Fig. 3f), which is believed to be more naïve with more ISCs presented in ISC organoids. To confirm this observation, we have therefore performed single-cell RNA sequencing (scRNA-seq) on both control and compressed organoids to provide a precise assessment at three levels: cell composition, gene expression, and signaling pathway activity. Compressed organoids showed increased proportions of stem cells and transit-amplifying (TA) cells (cells with the capability to differentiate into different types of intestinal epithelial cells), while the proportions of terminally differentiated secretory and absorptive cells were decreased compared to controls (Supplementary Fig. 3a). This demonstrates a clear shift toward a less differentiated cellular state. In compressed organoids, stemness-related genes such as *Lgr5* and *Smoc2*, as well as proliferation markers like *Mki67*, showed upregulated expression. Conversely, differentiation-associated genes were downregulated (Supplementary Fig. 3b, c). This gene expression profile is characteristic of a more primitive, stem-like state. Additionally, signaling pathways associated with cell proliferation were activated in compressed organoids, while pathways driving cell differentiation were inhibited (Supplementary Fig. 3d). This further confirms that volumetric compression maintains organoids in a more proliferative, less differentiated state.

Moreover, with additional CHIR in Og medium, the promotion effect of volumetric compression on the growth of intestinal organoid was consistently observed (Fig. 3g), due to the presence of endogenous Wnt ligands from Paneth cells in organoids. Practically, volumetric compression also enlarged both the area (Fig. 3h) and the diameter (Fig.3i) of the intestinal organoid, as well as led rounder morphology (Fig. 3j). These results suggested that the volumetric compression could synergize with other promotive small molecules such as CHIR to further augment the growth of intestinal organoids. Lgr5+ intestinal stem cells (ISCs) in organoids depend on active Wnt/β-catenin signaling for self-renewal and proliferation. Without exogenous Wnt3a (ISC medium) or the synergy between R-spondin supplementation (Og medium) and endogenous Wnt ligands from Paneth cells, healthy intestinal organoids undergo differentiation and apoptosis within days. This Wnt dependency is a fundamental characteristic of normal intestinal epithelium. Thus, for healthy intestinal organoids, only the ON state of Wnt signaling can guarantee the growth of healthy intestinal organoids.

As compared to intestinal organoids/epithelium, 70% of CRC patients display APC mutations within the Wnt/β-catenin pathway, resulting in constitutive β-catenin accumulation and pathway activation independent of upstream Wnt ligands and LRP6 receptors[53]. These CRC organoids can survive and proliferate without any exogenous Wnt supplementation—a hallmark of their transformed state. Moreover, there are no Paneth cells in CRC organoids, which means that there is no endogenous production of Wnt ligands. Thus, the CRC organoids naturally exist with an OFF state of Wnt signaling upstream activation. To absolutely confirm our CRC organoids were functioning independently of Wnt ligands, we have treated CRC organoids with IWP2 (Porcupine inhibitor that blocks all Wnt ligand secretion). We also conducted human WNT3A ELISA experiments to quantify endogenous Wnt3a in CRC organoid culture supernatant. Results showed Wnt3a protein concentration was near zero both with and without IWP2 treatment (Supplementary Fig. 4a). Targeting Wnt signaling and suppressing pathological β-catenin has long been viewed as a potential therapeutic approach for many related diseases, including CRC[45]. However, due to the widespread effect and essential role of canonical Wnt/β-catenin signaling in the development and homeostasis of many cell lineages and tissues, safely targeting Wnt signaling has rarely been achieved through biochemical or genetic means. Given the precise and multifaceted effect of volumetric compression on Wnt/β-catenin signaling via mechano-biochemical circuits, we hypothesized that this mechanical approach could suppress CRC growth without perturbing or even promoting other healthy tissues. Given the loss of function of Wnt ligands in CRC organoids due to mutated Wnt pathway, we suggested that the mechano-biochemical circuit switched to inverting input for inhibiting growth of CRC organoids (Fig. 3k). To test this hypothesis, we obtained patient-derived CRC organoids with APC mutations and subjected these organoids to volumetric compression. To confirm that the growth of patient-derived CRC organoids was independent of Wnt ligands, we also cultured CRC organoids with IWP2 treatment, which blocks endogenous Wnt ligand secretion and therefore prevents signaling upstream of complex formation[54]. The IWP2 treatment had no effect on CRC organoids (Fig.3l–p). To ensure no Wnt ligands were present in the culturing condition, IWP2 was added when we applied volumetric compression. Indeed, volumetric compression inhibited the growth of CRC organoids (Fig. 3l), as indicated by both the areas (Fig. 3m) and diameters of the organoids (Fig. 3n), and affected their morphology by roundness (Fig. 3o). Notably, volumetric compression with 3% PEG 300 solely inhibited the growth of CRC organoids without affecting the viability of cells in the organoids (Fig. 3p); a larger volumetric compression with 4% PEG 300 further inhibited the growth of CRC organoids but slightly reduced viability of cells (Fig. 3p).

Together, under the framework of mechano-biochemical circuit, volumetric compression promoted the growth of healthy intestinal organoids while suppressing the growth of patient-derived CRC organoids, thereby enabling the safe and precise targeting of Wnt signaling for cancer inhibition and the potential regeneration of healthy intestinal cells.

Volumetric compression interplays with Wnt/β-catenin signaling for regulation of intestinal epithelium

To further confirm that this regulation induced by volumetric compression is enabled by a phase-separation-driven mechano-biochemical circuit, we explored the activation of Wnt/β-catenin signaling and the importance of AXIN phase separation in the regulation of intestinal systems. First of all, WT AXIN-mCherry was delivered into CRC organoids via lentivirus to image the phase separation and condensate formation of AXIN under volumetric compression. In patient-derived CRC organoids, the FRAP assay had been conducted to confirm the dynamic feature of AXIN condensates (Fig. 4a). Additionally, we showed that volumetric compression promoted the formation of AXIN condensates in CRC organoids, with a larger fraction of AXIN observed in condensates under volumetric compression (Fig. 4b, c). In the next step, we further evaluated whether β-catenin was differentially regulated under volumetric compression between CRC organoids and healthy intestinal organoids. Within the context of CRC, where volumetric compression inhibited the growth of CRC organoids (Fig. 3k), our experiments showed that volumetric compression decreased the accumulated β-catenin in CRC organoids (Fig. 4d, e). By quantifying the intensity of total β-catenin per organoid, we found that volumetric compression from an additional 3% PEG 300 decreased total β-catenin by 5-fold, demonstrating its capability to efficiently inhibit the pathological accumulation of β-catenin in CRC. We also conducted both bulk and single-cell (sc) transcriptome profiling on CRC organoids with and without volumetric compression. Our results clearly showed that Wnt/β-catenin signaling was regulated under volumetric compression, as indicated by both the signature genes (Fig. 4f) and enriched GO/KEGG terms (Supplementary Fig. 4b). Additionally, the sc-seq assays also revealed a decrease in Wnt signaling-associated or target genes such as *AXIN2*, *MYC*, *CCND1*, *JUN*, *LGR5*, *PPARD*, *CTNNB1*, *SOX9*, and *WNT2B* in individual cells within the population (Fig. 4k, l). A Gene Set Enrichment Analysis (GSEA) also confirmed the downregulated canonical WNT pathway (Supplementary Fig. 4c).

In healthy intestinal epithelium, where volumetric compression promoted the growth of healthy intestinal organoids (Fig. 3a), our experiments showed that volumetric compression increased the accumulated β-catenin in both mouse healthy ISC spheroids (with ISC medium) (Fig. 4g, h) and intestinal organoids (with Og medium) (Fig. 4i, j). Given these evidences, we confirmed that the mechano-biochemical circuits regulated cell fate in healthy intestinal organoids and CRC organoid via differentially interfering with activation of Wnt/β-catenin signaling.

To further confirm that the phase separation based mechano-ochemical circuit happens in organoids under the operation of volumetric compression, we performed immunofluorescence imaging in two organoid systems representing distinct Wnt states. For the Wnt-ON model, the ISC organoids require active Wnt signaling for survival and represent a canonical Wnt-ON state. Under basal conditions, we observed AXIN condensates with some localization to the cell membrane. Following PEG compression treatment, AXIN condensates showed enhanced enrichment at the plasma membrane (Supplementary Fig. 5a, b), consistent with increased LRP6 signalosome formation as observed in our HEK293T experiments. For the Wnt-OFF model, the CRC organoids harbor APC mutations that disrupt the destruction complex, representing a state where β-catenin is constitutively accumulated downstream, but the upstream ligand-dependent machinery is non-functional. We observed AXIN condensates co-localizing with APC in the cytoplasm. Following PEG compression, the degree of AXIN-APC colocalization was further enhanced (Supplementary Fig. 5c, d), indicating increased destruction complex assembly, which is consistent with our observation that compression decreases β-catenin levels in CRC organoids (Fig. 4d, e).

Discussion

In summary, we propose a mechano-biochemical circuit via phase separation where mechanical signaling and biochemical pathways interplay within a hybrid microenvironment to direct cell fate. Currently, genetic synthetic circuits are primarily controlled by three types of triggers: chemical ligands (small molecules, ions, or proteins), endogenous metabolites, and light. In this paper, we introduce a mechanical element capable of constructing regulatory networks in genetic circuits to control biological processes and cell fate decisions. The mechano-biochemical circuit integrates mechanical and biochemical inputs to bidirectionally regulate Wnt signaling. We describe this as functionally analogous to an operational amplifier based on three properties: dual input integration, input-dependent mode switching (Wnt ligands determine inverting vs. non-inverting behavior), and signal amplification (compression enhances Wnt responses ~2-folds; Fig. 2h, i, n). This circuit-like information processing occurs through phase separation. The effect of this mechanical element is achieved through biomolecular phase separation: the degree of phase separation determines the strength of the signal transduction, while the subcellular translocation of phase-separated proteins functions as a switch to determine cellular outcomes. The importance of phase separation has been highlighted in both essential biological processes, such as gene expression and signaling transduction, and diverse pathological diseases, including cancer progression and development of neurodegenerative diseases. Among these processes, intracellular phase separations are often triggered by microenvironmental cues and stresses, such as various morphogens, pathogens, ions, and reactive oxygen species. In addition, our and others' previous researches also highlighted that the phase separable proteins can work as a mechanoregulator or transducer towards physical or mechanical perturbations in microenvironment. Since the previous literatures mainly reporting how protein phase separation responses towards a single type of stimuli, this study revealed a role of phase separation to process and compute complex microenvironmental cues with biochemical and mechanical informations, highlight its importance in development of organs and organisms, as well as its potential in engineering synthetic living systems.

Our findings reveal that cells sense mechanical forces not only through dedicated mechanosensor proteins but also through bulk physical changes in cellular organization. While classical mechanotransduction involves force-induced conformational changes in specific sensors (Piezo channels, integrins, YAP/TAZ), volumetric compression operates through altered thermodynamic landscapes for molecular interactions. Multiple physiological mechanical inputs—tissue crowding, osmotic gradients, matrix confinement, and tumor pressure—converge on reduced cellular volume and increased macromolecular crowding. Our demonstration that diverse mechanical perturbations (3D compression, substrate stiffness, stretch) produce similar effects on cell volume and Wnt signaling supports this convergence model. The mechanism operates through excluded volume effects: external forces drive water efflux, constraining macromolecules within smaller physical space and shifting equilibria for protein-protein interactions to favor phase separation. This volumetric mechanobiology complements sensor-based transduction, with phase separation serving as a critical molecular mediator linking physical constraint to biochemical outputs. Instead of identifying specific mechanoresponsive biomolecules, this study deciphers mechanoregulation from a system

https://doi.org/10.1038/s41467-025-68209-y

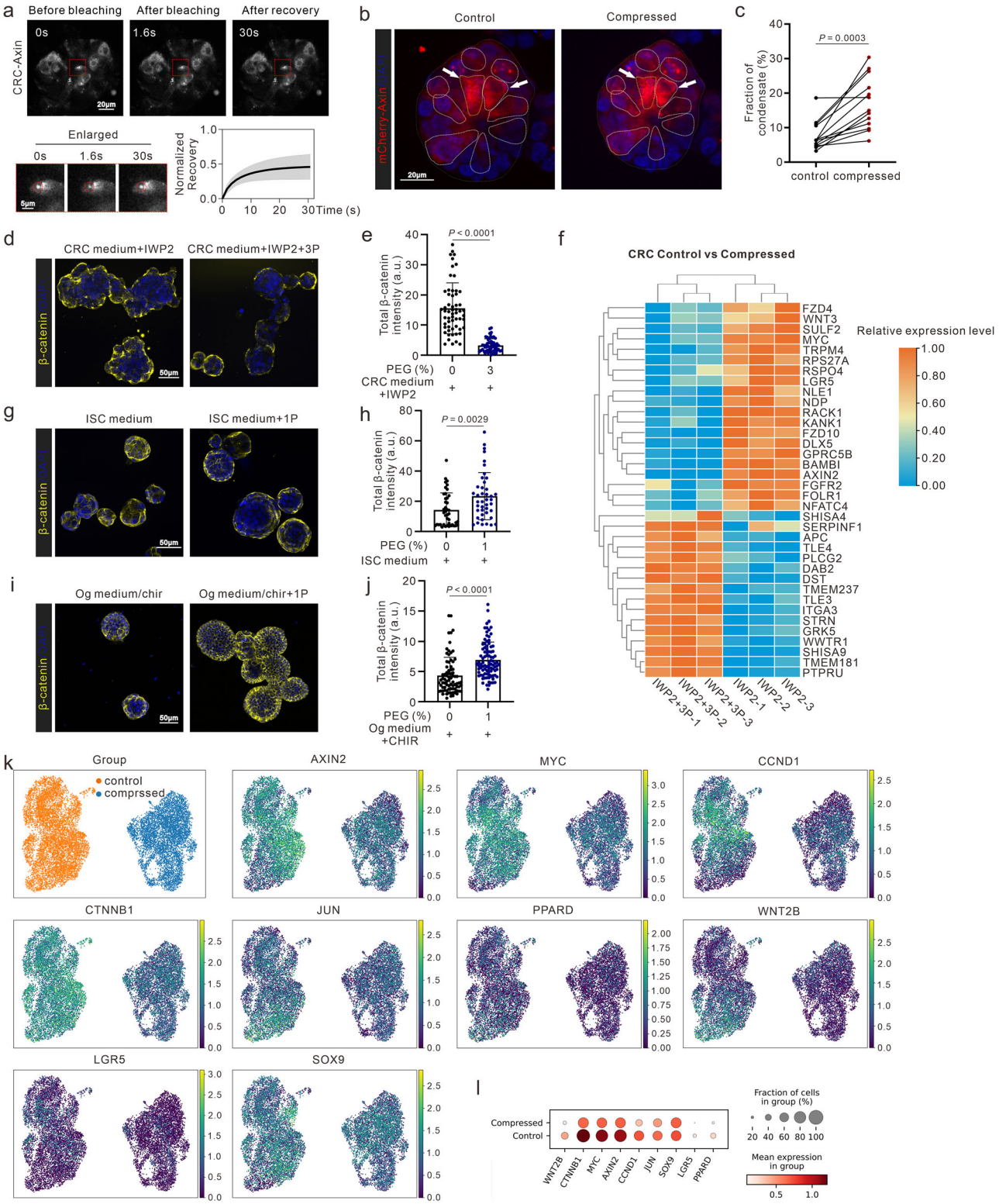

biology perspective. The mechano-biochemical circuit provides a framework to integrate currently known mechanical signaling pathways. In this study, the mechano-biochemical circuit controls the activation or suppression of Wnt/β-catenin signaling at the molecular level, induces the formation of either the LRP6 signalosome or the β-catenin destruction complex at the organelle level, and results in the growth or suppression of the intestinal epithelium at the multicellular tissue/organ level. Our study highlights the broad spectrum of cellular outcomes in response to physical or mechanical cues, emphasizing the urgent need for a systematic model to elucidate the regulatory network underlying cellular perception and response to mechanical signals.

Furthermore, our circuit specifically modulates the activation and suppression of Wnt/β-catenin signaling, achieving precise and safe targeting of this pathway. Wnt/β-catenin signaling is crucial in

Fig. 4 | The bidirectional regulation of Wnt by the mechano-biochemical operational amplifier is enabled by AXIN phase separation. a FRAP assay showing the recovery of AXIN condensates after photo-bleaching. Top panels show a larger field of view (Scale bar, 20 μm), and bottom panels show magnified views of the red boxed regions (Scale bar, 5 μm). Data are presented as mean ± s.d. ($n = 7$ biologically independent experiments). **b** Representative images showing AXIN condensates in the same CRC organoids before and after volumetric compression. White arrows indicate regions with distinct changes in droplets. Scale bar, 20 μm. **c** Quantification of fraction of total AXIN in condensates in CRC organoids before and after volumetric compression ($n = 13$ organoids). Data were analyzed by two-tailed paired *t*-test. In CRC organoids, volumetric compression inhibits β-catenin accumulation as indicated by representative immunofluorescence images (**d**) and quantification of intensity ($n = 58$ organoids per group) (**e**). **f** Heatmap of differentially expressed genes (DEGs) in CRC organoids before and after volumetric compression ($n = 3$ biologically independent samples per group). Color scale indicates normalized gene expression levels. In ISC spheroids, volumetric compression increases β-catenin accumulation as indicated by representative immunofluorescence images (**g**) and quantification of β-catenin intensity ($n = 42$ organoids per group) (**h**). In intestinal organoids, volumetric compression increases β-catenin accumulation as indicated by representative immunofluorescence images (**i**), and quantification β-catenin intensity (Control, $n = 79$; Compressed, $n = 92$ organoids) (**j**). scRNA-seq analysis of CRC organoids showing that Wnt signaling-associated genes such as *AXIN2*, *MYC*, *CCND1*, *JUN*, *LGR5*, *PPARD*, *CTNNB1*, *SOX9*, and *WNT2B* are downregulated under volumetric compression, visualized by UMAP feature plots (**k**) and quantified by mean gene expression (**l**). Color scale represents log-normalized gene expression. In **d**, **g**, **i**, scale bars, 50 μm. In **e**, **h**, **j**, data are presented as mean ± s.d. and were analyzed by two-tailed unpaired *t*-test. Exact *p* values are shown in the figure. Source data are provided as a Source Data file.

numerous developmental and homeostatic processes, impacting cell proliferation, differentiation, migration, genetic stability, apoptosis, and stemness maintenance. Aberrations in this pathway cause various diseases, including cancer, fibrosis, and neurodegeneration. Despite its significance, therapeutic molecules specifically targeting the Wnt pathway have only recently entered clinical trials, with none yet approved due to the challenge of precise and safe targeting. Here, we propose an alternative strategy to chemical ligands (e.g., small molecules, proteins, and ions) by employing mechanical stimuli to interfere with Wnt/β-catenin signaling in an orthogonal dimension. This approach simultaneously promotes canonical Wnt signaling and suppresses pathological β-catenin accumulation. Specifically, volumetric compression can differentially affect the intestinal epithelium by promoting the growth of healthy intestinal cells while suppressing the proliferation of CRC cells, due to the distinct activation mechanisms of Wnt/β-catenin signaling in these cells. This study highlights the potential of this mechano-biochemical circuit to enable mechanotherapy.

Beyond the intestinal epithelium, with a comprehensive understanding of the regulatory network in disease development, mechanotherapy can potentially be achieved by designing therapeutic circuits with mechanical inputs. Our current experimental approach employs global PEG 300-mediated compression, which differs from the spatially heterogeneous forces in native crypts. Nevertheless, intestinal epithelium experiences daily osmotic variations with a range of hundreds of mOsm[55–59], validating osmotic manipulation as physiologically relevant. Future studies incorporating spatial heterogeneity through microfluidic devices or in vivo imaging of condensate dynamics would provide valuable complementary insights into whether mechanical force patterns create cellular heterogeneity beyond biochemical niche factors. Overall, this proof-of-concept demonstration of a mechano-biochemical circuit provides a paradigm for understanding mechanoregulation from a system biology perspective. Moreover, it offers promising prospects for mechanotherapy, enabling precise treatments through the design of engineered regulatory circuits with mechanical inputs.

Methods

Cell culture

HEK293T cells (GNHu17) and RKO cells (TCHu116) were purchased from National Collection of Authenticated Cell Cultures (NCACC). Mouse L cells (CRL-2648), L Wnt-3A cells (CRL-2647) and L-WRN cells (CRL-3276) were obtained from American Type Culture Collection (ATCC). All cell lines were authenticated by the suppliers using STR profiling and tested negative for mycoplasma contamination. HEK293T cells and RKO cells were maintained in DMEM (Gibco) supplemented with 10% FBS (Gibco) at 37 °C in a humidified, 5% CO2 incubator. Mouse L cells and L Wnt3A cells were used for preparation of control and Wnt3A conditioned medium according to ATCC protocol. L-WRN cells were used to collect WRN conditioned medium for murine organoid culture.

CRISPR/Cas9 genome editing and plasmid construction

HEK293T and RKO cells were transfected with plasmids encoding Cas9 and a single-guide RNA (sgRNA: 5′-TTCGCTGTACCGTCTACTGG-3′; targeting exon 1 of the *AXIN1* gene) using Lipo8000 (Beyotime C0533). Following transfection, cells expressing Cas9 and sgRNA were selected using puromycin. Western blot analysis was performed to assess AXIN1 protein expression levels, and genomic PCR followed by Sanger sequencing was conducted to verify mutations at the target site. Two *AXIN1* knockout clones (KO1 and KO2) with high knockout efficiency were obtained and used in this study. The mCherry-AXIN1ΔDAX mutant plasmid was generated by deleting the DAX domain (amino acids 746-862) from the full-length AXIN1 plasmid using standard cloning techniques. All unique plasmids and stable cell lines generated in this study are available from the corresponding author upon reasonable request.

Lentivirus production and transduction

Lentiviral particles expressing mCherry-AXIN1 or mCherry-AXIN1ΔDAX were generated in HEK293T cells by co-transfection of the plasmids with the third-generation lentivirus packaging vectors (psPAX2 and pMD2.G). Forty-eight hours after transfection, the supernatant was collected and filtered. When AXIN1-KO RKO cells were approximately 70% confluence, the supernatant was added to the medium for 24 h of infection. Stably transduced cell lines were obtained by 2–3 rounds of puromycin selection. For CRC organoids stably expressing mCherry-AXIN1, the filtered supernatant was ultracentrifuged at 80,000 × *g* for 2 h at 4 °C, and the pellet was resuspended in CRC medium. CRC organoids were cultured as two-dimensional monolayers on Matrigel and incubated with the viral medium for 24 h. Stably transduced CRC organoids were achieved through 2–3 rounds of puromycin selection.

Fluorescence recovery after photo-bleaching (FRAP)

To investigate the diffusion dynamics of mCherry-AXIN1, FRAP experiments were performed on a Fluoview FV3000 confocal laser scanning microscope equipped with a 100×UPLSAPO oil immersion objective (NA 1.4; Olympus). A region of interest (ROI) within an mCherry-AXIN1 condensate in HEK293T cells was selected and bleached using a 594 nm laser at 100% intensity. Time-lapse images were acquired at an interval of 10.8 ms between frames. In CRC organoids, images were captured every 16.1 ms. To analyze fluorescence recovery kinetics, FRAP analysis was completed using the ImageJ FRAP Profiler plugin (Hardin lab:https://worms.zoology.wisc.edu/research/4d/4d.html#frap). The FRAP curves were generated using GraphPad Prism (v9.0), and the half-time of recovery ($t_1/_2$) was calculated by fitting the curve with a one-phase association function.

Osmotic stress

To induce cellular volume compression, PEG300 was added to the isotonic culture medium. Generally, we typically used a 2% PEG300 (v/v) concentration and stimulated cells for short periods (1–2 min) or prolonged periods (e.g., 12 h for gene expression assays, or up to several days for growth assays). To minimize potential osmotic shock and cellular damage, the PEG 300-containing hypertonic medium was added gently and gradually to the culture vessel. For organoid experiments, human CRC organoids were treated with 3% (v/v) PEG300, while murine ISC organoid were treated with 1% (v/v) PEG300. To investigate the dynamic response of AXIN1 condensates to osmotic stress, a 2D organoid monolayer culture system was established. Briefly, confocal dishes were pre-coated with 25 μL of Matrigel and incubated at 37 °C for 30 min for polymerization. CRC organoids were dissociated and seeded onto the Matrigel to form a confluent monolayer. Osmotic stress was induced by adding 3% (v/v) PEG300 to the culture medium, followed immediately by time-lapse imaging.

Immunoblotting and co-immunoprecipitation (Co-IP)

For immunoblotting, cell lysates were prepared on ice with the RIPA lysis buffer. For the preparation of cytosolic proteins, cells were lysed with 0.015% digitonin in PBS containing a cocktail of protease inhibitors. Lysates were centrifuged at 12,000 × *g* for 10 min, and the supernatants were collected, separated by 10% SDS-PAGE, and transferred to polyvinylidene fluoride (PVDF) membranes. After blocking with QuickBlock buffer for 15 min at room temperature, the membranes were incubated with primary antibodies overnight at 4 °C and followed by secondary antibodies IRDye 800CW goat anti-mouse IgG and/or IRDye 680LT goat anti-rabbit IgG (LI-COR Biosciences; 1:10,000 dilution) for 1 h at room temperature. Signals were detected using the Odyssey CLx Imaging System (LI-COR Biosciences) and analyzed with Fiji (ImageJ v1.54f). For Co-IP, HEK293T cells were lysed on ice with NP40 lysis buffer (50 mM Tris-HCl, pH 7.4, 150 mM NaCl, 0.5% NP-40,1.5 mM MgCl2, 10% glycerol and protease inhibitors). Lysates were centrifuged at 12,000 × *g*, and after taking an aliquot for total protein expression analysis, immunoprecipitation was performed by adding BeyoMag™ Anti-Flag Magnetic Beads to the remaining cell lysate followed by incubation at 4 °C overnight with gentle rotation. The immune complex was isolated by 16-Tube SureBeads™ Magnetic Rack (Bio-Rad), washed three times with lysis solution, eluted by boiling in SDS sample buffer, and analyzed by SDS-PAGE and immunoblotting. Uncropped scans of blots are provided in the Source Data file. Detailed information regarding antibody sources, catalog numbers, and dilutions is provided in Supplementary Table 1, while commercial reagents and their corresponding supplier details are listed in Supplementary Table 2.

Immunofluorescence (IF)

For cell immunofluorescence, cells were fixed in 4% paraformaldehyde (PFA) for 15 min at room temperature, washed three times with cold PBS (5 min each time), blocked in 5% BSA in PBS containing 0.3% TritonX-100 at room temperature for 1 h, and incubated with primary antibodies at 4 °C overnight. After removing primary antibodies and washing with PBS, cells were treated with secondary antibodies for 1 h at room temperature. After thorough washing, the stained cells were visualized using a spinning disk confocal microscope. For organoid immunofluorescence, murine ISC colonies or human CRC organoids embedded in Matrigel were fixed in 4% PFA for 30 min at room temperature. Suspended tissues were collected and centrifuged 500 × *g* for 5 min to remove the PFA, washed with ultra-pure water and pelleted. Following resuspension in water, the organoids were spread on 20-mm glass-bottom culture dishes and allowed to attach by air-drying. Attached organoids were rehydrated and blocked in 5% BSA in PBS containing 0.3% Triton X-100 at 4 °C for 48 h, and incubated with primary antibodies at 4 °C for 48 h. After removal of primary antibodies and washing with PBS for at least 3 h, samples were incubated with secondary antibody at 4 °C for 24 h. Following extensive washing, the samples were imaged with confocal microscopy. Detailed information regarding antibody sources, catalog numbers, and dilutions is provided in Supplementary Table 1.

Reverse transcription quantitative PCR (RT-qPCR)

Total RNA was extracted from RKO cells using Qiagen RNeasy mini kit and converted to cDNA with HiScript III All-in-one RT SuperMix Perfect for qPCR. RT-qPCR was performed on an Agilent AriaMx 96 Real-Time PCR System using Taq Pro Universal SYBR qPCR Master Mix. The relative expression levels of target genes (*AXIN2*, *LEF1*, and *SP5*) were normalized to that of the housekeeping gene GAPDH using the $2^{-\Delta\Delta Ct}$ method. The sequences of all primers used in this study are listed in Supplementary Table 3.

Intestinal crypt isolation

Murine intestinal crypts were isolated from 6-week-old male C57BL/6J mice obtained from Shulaibao (Wuhan) Biotechnology Company. Mice were housed in a specific pathogen-free (SPF) facility under a standard 12-h light/12-h dark cycle, with a controlled ambient temperature of 22 ± 2 °C and relative humidity of 40–60%. Male mice were selected to minimize potential experimental variability, although the isolation protocol is applicable to both sexes. Briefly, the proximal part of the intestines was isolated, opened longitudinally, and gently scraped to remove luminal contents and villi using a glass slide. The intestinal tissue was chopped into 1 to 2 mm pieces and washed 12–15 times with ice-cold PBS until the supernatant was clear. Crypts were released by incubating intestinal pieces in ice-cold 2 mM EDTA in PBS for 30 min at room temperature. The digested tissue was then resuspended and shaken vigorously to liberate the crypts. The supernatant was collected and passed through a 70-μm strainer for enrichment. The crypt fraction was centrifuged at 290 × *g* for 5 min at 4 °C to remove single cells and debris. The enriched crypts were embedded in Matrigel.

Organoid culture

Murine intestinal crypts and human CRC organoids were embedded in Matrigel and dispensed as 50 μL droplets in 24-well plates. After polymerization for 30 min at 37 °C, the gels were overlaid with 500 μL of culture medium. For murine organoids, the culture medium consisted of Advanced DMEM/F12 supplemented with Glutamax, HEPES, penicillin-streptomycin, B27, N2, and N-acetylcysteine, as well as growth factors including EGF, Noggin, Wnt3a, and R-spondin (conditioned medium from mouse L-WRN cells). To generate differentiated intestinal organoids, Wnt3a was omitted from the culture medium to induce maturation. For human CRC organoid culture, the complete medium consisted of Advanced DMEM/F12 supplemented with Glutamax, HEPES, penicillin-streptomycin, B27, N2, N-acetylcysteine, EGF, A83-01, SB202190, and [Leu15]-Gastrin I. Detailed information including supplements and inhibitors are listed in Supplementary Table 2.

Transcriptome and single-cell sequencing

Bulk RNA-seq was performed on human CRC organoids, and scRNA-seq was performed on both human CRC organoids and murine small intestinal organoids. In all experiments, organoids were treated with or without PEG 300. Sequencing services were provided by Tsingke Biotechnology for bulk RNA-seq, Mozhuo Biotech for human scRNA-seq, and Seek Gene for murine scRNA-seq. Differential expression analysis for bulk RNA-seq was performed using DESeq2 in R. Single-cell data matrices were processed and analyzed using Scanpy in Python, including quality control, dimensionality reduction, and clustering.

Statistics and reproducibility

Statistical analyses were performed using GraphPad Prism (v9.0). Data are presented as mean ± standard deviation (s.d.) with individual data

points shown where applicable. Comparisons between two groups were performed using unpaired or paired two-tailed Student's *t* test, ratio paired *t*-test, or one-sample *t*-test for normalized data, as indicated in the figure legends. For comparisons among more than two groups, one-way analysis of variance (ANOVA) or the Kruskal–Wallis test (for non-normally distributed data) was employed, followed by Tukey's or Dunn's multiple comparisons test, respectively. Exact *p* values are indicated on the figures, and values less than 0.05 were considered statistically significant. For Western blot analysis, band intensities were quantified using Fiji (ImageJ v1.54f). For Co-IP experiments, densitometry data were analyzed using raw ratios or normalized values as specified. Source data are provided as a Source Data file. No statistical method was used to predetermine sample size. No data were excluded from the analyses. The experiments were not randomized. The Investigators were not blinded to allocation during experiments and outcome assessment. All experiments were repeated at least three times independently with similar results, unless otherwise stated.

Ethics statement

The study involving human participants was conducted in strict accordance with the Declaration of Helsinki. Ethical approval was granted by the Medical Ethics Committee of Union Hospital, Tongji Medical College, Huazhong University of Science and Technology (Approval No. 2024-0112) and the Medical Ethics Committee of Tongji Medical College, Huazhong University of Science and Technology (Approval No. 2024-S163). Written informed consent was obtained from all patients.

All animal experiments were performed in strict accordance with the relevant ethical regulations and were approved by the Animal Care and Use Committee (IACUC) of Huazhong University of Science and Technology (Protocol No. 4151).

Reporting summary

Further information on research design is available in the Nature Portfolio Reporting Summary linked to this article.

Data availability

The raw sequence data reported in this paper have been deposited in the Genome Sequence Archive in the National Genomics Data Center, China National Center for Bioinformation/Beijing Institute of Genomics, Chinese Academy of Sciences. Specifically, the single-cell RNA-seq data for human colorectal cancer organoids are accessible in GSA-Human under accession codes HRA015319 and HRA013862, and the bulk RNA-seq data are accessible under accession code HRA013863. The single-cell RNA-seq data for murine organoids are accessible under accession code CRA032833. All unique materials and stable cell lines generated in this study are available from the corresponding author upon reasonable request. All other data supporting the findings of this study are available within the article and its Supplementary Information. Source data are provided with this paper.

References

1. Li, Y., Tang, W. & Guo, M. The cell as matter: connecting molecular biology to cellular functions. *Matter* **4**, 1863–1891 (2021).
2. Li, Y., Wong, I. Y. & Guo, M. Reciprocity of cell mechanics with extracellular stimuli: emerging opportunities for translational medicine. *Small* **18**, 2107305 (2022).
3. Du, H. et al. Tuning immunity through tissue mechanotransduction. *Nat. Rev. Immunol.* **23**, 174–188 (2023).
4. Romani, P., Valcarcel-Jimenez, L., Frezza, C. & Dupont, S. Crosstalk between mechanotransduction and metabolism. *Nat. Rev. Mol. Cell Biol.* **22**, 22–38 (2021).
5. Saraswathibhatla, A., Indana, D. & Chaudhuri, O. Cell–extracellular matrix mechanotransduction in 3D. *Nat. Rev. Mol. Cell Biol.* **24**, 495–516 (2023).
6. Di, X. et al. Cellular mechanotransduction in health and diseases: from molecular mechanism to therapeutic targets. *Signal Transduct. Target. Ther.* **8**, 282 (2023).
7. Shyer, A. E. et al. Emergent cellular self-organization and mechanosensation initiate follicle pattern in the avian skin. *Science* **357**, 811–815 (2017).
8. Segel, M. et al. Niche stiffness underlies the ageing of central nervous system progenitor cells. *Nature* **573**, 130–134 (2019).
9. Li, Y. et al. Compression-induced dedifferentiation of adipocytes promotes tumor progression. *Sci. Adv.* **6**, eaax5611 (2020).
10. Blache, U. et al. Engineered hydrogels for mechanobiology. *Nat. Rev. Methods Prim.* **2**, 98 (2022).
11. Benham-Pyle, B. W., Pruitt, B. L. & Nelson, W. J. Mechanical strain induces E-cadherin–dependent Yap1 and β-catenin activation to drive cell cycle entry. *Science* **348**, 1024–1027 (2015).
12. Fernandez-Sanchez, M. E. et al. Mechanical induction of the tumorigenic β-catenin pathway by tumour growth pressure. *Nature* **523**, 92–95 (2015).
13. Li, Y. et al. Volumetric compression induces intracellular crowding to control intestinal organoid growth via Wnt/β-catenin signaling. *Cell Stem Cell* **28**, 63–78.e67 (2021).
14. Jansen, J. H. et al. Stretch-induced inhibition of Wnt/β-catenin signaling in mineralizing osteoblasts. *J. Orthop. Res.* **28**, 390–396 (2010).
15. Andreu, I. et al. Mechanical force application to the nucleus regulates nucleocytoplasmic transport. *Nat. Cell Biol.* **24**, 896–905 (2022).
16. Esposito, D. et al. ROCK1 mechano-signaling dependency of human malignancies driven by TEAD/YAP activation. *Nat. Commun.* **13**, 703 (2022).
17. Totaro, A. et al. YAP/TAZ link cell mechanics to Notch signalling to control epidermal stem cell fate. *Nat. Commun.* **8**, 15206 (2017).
18. Xue, X. et al. Mechanics-guided embryonic patterning of neuroectoderm tissue from human pluripotent stem cells. *Nat. Mater.* **17**, 633–641 (2018).
19. Wang, N., Butler, J. P. & Ingber, D. E. Mechanotransduction across the cell surface and through the cytoskeleton. *Science* **260**, 1124–1127 (1993).
20. Moroni, M., Servin-Vences, M. R., Fleischer, R., Sánchez-Carranza, O. & Lewin, G. R. Voltage gating of mechanosensitive PIEZO channels. *Nat. Commun.* **9**, 1096 (2018).
21. Dupont, S. et al. Role of YAP/TAZ in mechanotransduction. *Nature* **474**, 179–183 (2011).
22. Li, P. et al. High-throughput and proteome-wide discovery of endogenous biomolecular condensates. *Nat. Chem.* **16**, 1101–1112 (2024).
23. MacDonald, B. T., Tamai, K. & He, X. Wnt/β-catenin signaling: components, mechanisms, and diseases. *Dev. Cell* **17**, 9–26 (2009).
24. Müller, I. E. et al. Gene networks that compensate for crosstalk with crosstalk. *Nat. Commun.* **10**, 4028 (2019).
25. Ahrends, R. et al. Controlling low rates of cell differentiation through noise and ultrahigh feedback. *Science* **344**, 1384–1389 (2014).
26. Zhu, R., del Rio-Salgado, J. M., Garcia-Ojalvo, J. & Elowitz, M. B. Synthetic multistability in mammalian cells. *Science* **375**, eabg9765 (2022).
27. Xie, M. & Fussenegger, M. Designing cell function: assembly of synthetic gene circuits for cell biology applications. *Nat. Rev. Mol. Cell Biol.* **19**, 507–525 (2018).
28. Bahrami-Nejad, Z. et al. A transcriptional circuit filters oscillating circadian hormonal inputs to regulate fat cell differentiation. *Cell Metab.* **27**, 854–868.e858 (2018).
29. Bonnet, J., Yin, P., Ortiz, M. E., Subsoontorn, P. & Endy, D. Amplifying genetic logic gates. *Science* **340**, 599–603 (2013).
30. Zhou, Z. et al. Engineering longevity—design of a synthetic gene oscillator to slow cellular aging. *Science* **380**, 376–381 (2023).

31. Bienz, M. Head-to-tail polymerization in the assembly of biomolecular condensates. *Cell* **182**, 799–811 (2020).
32. Nong, J. et al. Phase separation of Axin organizes the β-catenin destruction complex. *J. Cell Biol.* **220**, e202012112 (2021).
33. Wang, Y. et al. USP10 strikes down β-catenin by dual-wielding deubiquitinase activity and phase separation potential. *Cell Chem. Biol.* **30**, 1436–1452.e1410 (2023).
34. Fiedler, M., Mendoza-Topaz, C., Rutherford, T. J., Mieszczanek, J. & Bienz, M. Dishevelled interacts with the DIX domain polymerization interface of Axin to interfere with its function in down-regulating β-catenin. *Proc. Natl. Acad. Sci. USA* **108**, 1937–1942 (2011).
35. Schwarz-Romond, T. et al. The DIX domain of dishevelled confers Wnt signaling by dynamic polymerization. *Nat. Struct. Mol. Biol.* **14**, 484–492 (2007).
36. Wang, S. et al. Small-molecule modulation of Wnt signaling via modulating the Axin-LRP5/6 interaction. *Nat. Chem. Biol.* **9**, 579–585 (2013).
37. Stamos, J. L. & Weis, W. I. The β-catenin destruction complex. *Cold Spring Harb. Perspect. Biol.* **5**, a007898 (2013).
38. Bilic, J. et al. Wnt induces LRP6 signalosomes and promotes dishevelled-dependent LRP6 phosphorylation. *Science* **316**, 1619–1622 (2007).
39. Zeng, X. et al. A dual-kinase mechanism for Wnt co-receptor phosphorylation and activation. *Nature* **438**, 873–877 (2005).
40. Kim, S.-E. et al. Wnt stabilization of β-catenin reveals principles for morphogen receptor-scaffold assemblies. *Science* **340**, 867–870 (2013).
41. Li, V. S. et al. Wnt signaling through inhibition of β-catenin degradation in an intact Axin1 complex. *Cell* **149**, 1245–1256 (2012).
42. Hernández, A. R., Klein, A. M. & Kirschner, M. W. Kinetic responses of β-catenin specify the sites of Wnt control. *Science* **338**, 1337–1340 (2012).
43. Liu, C. et al. Control of β-catenin phosphorylation/degradation by a dual-kinase mechanism. *Cell* **108**, 837–847 (2002).
44. Morin, P. J. et al. Activation of β-catenin-Tcf signaling in colon cancer by mutations in β-catenin or APC. *Science* **275**, 1787–1790 (1997).
45. Kahn, M. Can we safely target the WNT pathway? *Nat. Rev. Drug Discov.* **13**, 513–532 (2014).
46. Law, S. M. & Zheng, J. J. Premise and peril of Wnt signaling activation through GSK-3β inhibition. *Iscience* **25**, 104159 (2022).
47. Ring, D. B. et al. Selective glycogen synthase kinase 3 inhibitors potentiate insulin activation of glucose transport and utilization in vitro and in vivo. *Diabetes* **52**, 588–595 (2003).
48. Batlle, E. et al. β-Catenin and TCF mediate cell positioning in the intestinal epithelium by controlling the expression of EphB/ephrinB. *Cell* **111**, 251–263 (2002).
49. De Lau, W. et al. Lgr5 homologues associate with Wnt receptors and mediate R-spondin signalling. *Nature* **476**, 293–297 (2011).
50. Sato, T. et al. Paneth cells constitute the niche for Lgr5 stem cells in intestinal crypts. *Nature* **469**, 415–418 (2011).
51. Valenta, T. et al. Wnt ligands secreted by subepithelial mesenchymal cells are essential for the survival of intestinal stem cells and gut homeostasis. *Cell Rep.* **15**, 911–918 (2016).
52. Yin, X. et al. Niche-independent high-purity cultures of Lgr5+ intestinal stem cells and their progeny. *Nat. Methods* **11**, 106–112 (2014).
53. Jorissen, R. N. et al. Wild-type APC predicts poor prognosis in microsatellite-stable proximal colon cancer. *Br. J. Cancer* **113**, 979–988 (2015).
54. Garcia-Reyes, B. et al. Discovery of inhibitor of Wnt production 2 (IWP-2) and related compounds as selective ATP-competitive inhibitors of casein kinase 1 (CK1) δ/ε. *J. Med. Chem.* **61**, 4087–4102 (2018).
55. Ichiki, T. et al. Sensory representation and detection mechanisms of gut osmolality change. *Nature* **602**, 468–474 (2022).
56. Li, Y. & Guo, M. Volumetric compression for engineering living systems. *Nat. Rev. Bioeng.* **2**, 1023–1038 (2024).
57. Ng, K. M. et al. Single-strain behavior predicts responses to environmental pH and osmolality in the gut microbiota. *MBio* **14**, e00753–00723 (2023).
58. Tropini, C. et al. Transient osmotic perturbation causes long-term alteration to the gut microbiota. *Cell* **173**, 1742–1754.e1717 (2018).
59. Zimmerman, C. A. et al. A gut-to-brain signal of fluid osmolarity controls thirst satiation. *Nature* **568**, 98–102 (2019).

Acknowledgements

We gratefully acknowledge the financial support from the National Key Research and Development Program of China (2024YFF1207300 to Y.L.), the National Natural Science Foundation of China (Grant numbers 32171248 to Y.L., 12472319 to Y.L.), the Fundamental Research Funds for Central Universities, HUST (2021GCRC056 to Y.L.).

Author contributions

Conceptualization: Y.L.; Methodology: Y.L., J.S., L.W., P.L., F.Q., M.L., L.X., C.S., Y. Zheng, and Y. Zhang; Investigation: J.S., Y.L., X.R., H.X., and W.W.; Visualization: J.S., Y.L., and P.C.; Funding acquisition: Y.L.; Project administration: Y.L.; Supervision: Y.L. and B.F.L.; Writing—original draft: Y.L. and J.S.; Writing—review & editing: Y.L., J.S., and B.F.L.

Competing interests

The authors declare no competing interests.

Additional information

Supplementary information The online version contains supplementary material available at https://doi.org/10.1038/s41467-025-68209-y.

Correspondence and requests for materials should be addressed to Yiwei Li.

Peer review information *Nature Communications* thanks Danfeng Cai and Shige Yoshimura for their contribution to the peer review of this work. A peer review file is available.